JOURNAL OF COMPUTATIONAL PHYSICS 119, 149–155 (1995)

A More Accurate Scharfetter–Gummel Algorithm of Electron Transport for Semiconductor and Gas Discharge Simulation

A. A. KULIKOVSKY

Institute for High Temperatures, Russian Academy of Sciences, Izhorskaya 13/19, Moscow, 127412, Russia

Received April 15, 1994; revised November 29, 1994

A well-known Scharfetter–Gummel (SG) scheme for convection-dominated problems of semiconductor and gas discharge plasmas is improved. A one-dimensional convection–diffusion equation is considered. It is shown that the original SG scheme is accurate if the potential drop between two adjacent nodes is much less than the electron temperature. To satisfy this condition a pair of additional nodes between adjacent nodes are inserted. The distance between these "virtual" nodes can be choosen small enough to obtain flux at the cell bound with the high accuracy. The number densities at virtual nodes are found by interpolation. Tests have shown that the accuracy of this scheme is comparable to the FCT technique, but in contrast it does not produce a "staircase" disturbance on rapidly changing functions.

1. INTRODUCTION

In this paper we will consider algorithm for the numerical solution of one-dimensional convection–diffusion equation

$$\frac{\partial n}{\partial t} + \frac{\partial j}{\partial x} = 0, \tag{1}$$

where n is the electron number density and

$$j = -D\frac{\partial n}{\partial x} - \mu E n \tag{2}$$

is the electron current density. Here D is the diffusion coefficient, μ is the mobility, and E is the electric field strength. *Throughout this paper we consider that* $\mu = const$.

Equation (1) is of great importance in various fields. Probably most frequently it occurs in semiconductor and gas discharge plasma simulation. In both cases it is used when hydrodynamic description of the electron transport is valid and one can neglect inertial terms in the momentum balance of electrons (2). Usually (1) is nonlinear due to the fact that the drift velocity of electrons $W = -\mu E$ depends on their number density via the Poisson equation.

In many situations Eq. (1) describes ion transport as well. However, for convenience throughout this paper we will refer to this equation as that of the electron mass balance.

The main difficulty is that n may change very rapidly—for several orders of magnitude within the computational domain. However, it is necessary to describe the transport of low values of n with the same accuracy as those of large n. This requirement is related to the fact that usually the source terms are presented in the right-hand side of (1). These sources strongly depend on electron density and can be high in the region where n is low. Thus the low values of n can essentially affect the accuracy of the whole solution [1].

In 1969 Scharfetter and Gummel [2] proposed a scheme for the numerical solution of (1). Their scheme, which will be referred as SG, is based on the following idea. Consider a computational cell between the half-integer points $k - \frac{1}{2}$ and $k + \frac{1}{2}$ (Fig. 1).

To obtain the expression for current density at the cell bound, say $j_{k+1/2}$, it is anticipated that between two nodes, k and $k + 1$, E, D, and j are constant and equal to $E_{k+1/2}$, $D_{k+1/2}$, and $j_{k+1/2}$. Then (2) is considered as a differential equation with respect to n on the interval (x_k, x_{k+1}). Solving this equation one obtains

$$n(x) = \left(n_k - \frac{j_{k+1/2}h_k}{D_{k+1/2}} \cdot \int_0^{\xi} e^{\alpha\xi'}\, d\xi'\right) e^{-\alpha\xi}, \tag{3}$$

where $h_k = x_{k+1} - x_k$, $\xi = (x - x_k)/h_k$, and

$$\alpha = \frac{\mu h_k E_{k+1/2}}{D_{k+1/2}}$$

Setting $x = x_{k+1}$ (thus $\xi = 1$) in (3), we come to the required expression for $j_{k+1/2}$,

$$j_{k+1/2} = \frac{D_{k+1/2}}{h_k I_0}(n_k - e^{\alpha} n_{k+1}), \tag{4}$$

where

0021-9991/95 $6.00

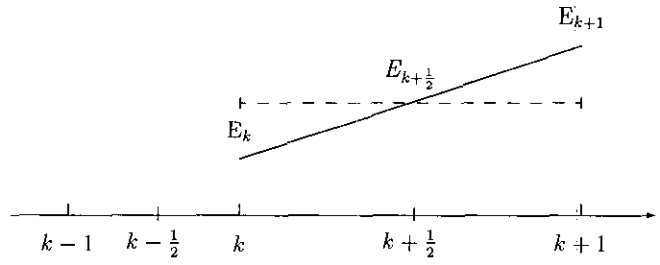

FIG. 1. Nodes designation.

$$I_0 = \frac{e^{\alpha} - 1}{\alpha}.$$

Then the solution of (1) can be obtained using, for example, the scheme

$$\frac{n_k^{m+1} - n_k^m}{\tau} = -\frac{j_{k+1/2}^m - j_{k-1/2}^m}{h_{k-1/2}}, \tag{5}$$

where m labels the time level and $S_{k+1/2} = \frac{1}{2}(S_k + S_{k+1})$, S being D, E, h.

Scheme (4), (5) has a very important property of monotonicity [3]. Since the pioneering work of Scharfetter and Gummel this scheme and its two-dimensional variant was widely used in semiconductor device simulation (see [4] and the literature cited there). It was introduced to gas discharge physics by Boeuf and Pitchford [5, 6], who applied an implicit variant of this scheme to simulate 2D pseudospark discharge and glow discharge in cylindrical geometry.

In this paper we first will consider generalization of the Scharfetter–Gummel scheme to a linear field. It will be shown that the original scheme is accurate if the potential drop between two adjacent nodes is much less than the electron temperature. This condition can be very restrictive. To avoid using fine grids, the following procedure is proposed.

Between two adjacent nodes a pair of additional nodes are inserted in such a way that the distance between them obeys the required condition. Densities in these "virtual" nodes are obtained using interpolation. Then the current density is calculated by (4), where the appropriate parameters are taken in the virtual nodes. This procedure dramatically improves the accuracy of the scheme.

The paper organization is as follows. In Section 2 the generalization of the Scharfetter–Gummel algorithm to the linear field is described. The space step limitation mentioned above is obtained. Then the virtual nodes are introduced in order to satisfy this requirement. Subsection 2.4 contains a brief formulation of improved Scharfetter–Gummel (ISG) scheme. Section 3 displays the results of a test problem solution. The ISG algorithm is compared with the exact solution and with the result obtained by the simple SG and flux-corrected transport (FCT) scheme. Some details of ISG realization are discussed.

2. DESCRIPTION OF THE SCHEME

2.1. *The Linear Field*

Consider the field being linear between two adjacent nodes, k and $k + 1$. Let $E_k \neq 0$. Field $E(x)$ then can be represented as

$$E(x) = E_k(1 + 2\beta\xi), \tag{6}$$

where $\xi = (x - x_k)/h_k$ and

$$\beta = \frac{\Delta E_k}{2E_k}, \quad \Delta E_k = E_{k+1} - E_k. \tag{7}$$

Solving Eq. (2) with constants $j_{k+1/2}$, $D_{k+1/2}$ and linear $E(x)$, Eq. (6), we come to

$$n(x) = \left[n_k - \frac{j_{k+1/2} h_k}{D_{k+1/2}} \int_0^{\xi} \exp\{f(\xi')\} d\xi' \right] \exp\{-f(\xi)\}, \tag{8}$$

where

$$f(y) = \alpha(y + \beta y^2) \tag{9}$$

and

$$\alpha = \frac{\mu h_k E_k}{D_{k+1/2}}.$$

Comparison of (3) and (8) shows that if the field is constant, (8) reduces to (3) if one puts $\beta = 0$ in (9). We conclude that the linear field gives an additional exponent $\exp(\alpha\beta y^2)$ in (8). As $y < 1$ this exponent can be expanded as a power series in the $\alpha\beta$ product, provided that condition $|\alpha\beta| \ll 1$ is satisfied. Retaining the first-order term we receive

$$e^{f(y)} \simeq e^{\alpha y}(1 + \alpha\beta y). \tag{10}$$

This procedure is valid, provided that the inequality

$$|\alpha\beta| = \frac{\mu h_k |\Delta E_k|}{2D_{k+1/2}} \ll 1$$

or

$$h_k \ll \frac{2D_{k+1/2}}{\mu |\Delta E_k|} \tag{11}$$

is satisfied. Noting that the diffusion coefficient is expressed in terms of the electron temperature via the Einstein relation $D = \mu T$, (11) can be rewritten as

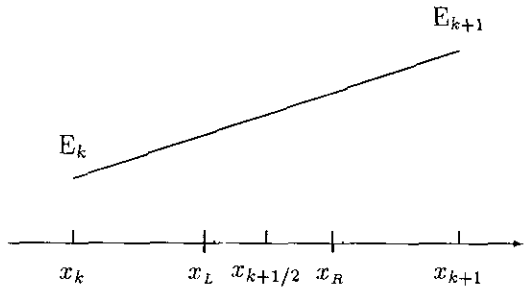

FIG. 2. Position of virtual nodes x_L and x_R.

$$\frac{|\Delta E_k| h_k}{2T_k} \ll 1. \tag{12}$$

We see that in terms of physical quantities (11) means that the electric potential drop between two adjacent nodes should be much less than the electron temperature. Condition (11) defines the accuracy of the scheme. If (11) is not satisfied, the solution obtained by the Scharfetter–Gummel scheme exhibits excessive diffusion smoothing.

Taking into account (10), from (8) we obtain

$$j_{k+1/2} = \frac{E_{k+1/2}}{h_k I_1} [n_k - e^{\alpha}(1 + \alpha\beta) n_{k+1}], \tag{13}$$

where

$$I_1 = \int_0^1 e^{\alpha y}(1 + \alpha\beta y^2)\, dy. \tag{14}$$

This integral can be calculated explicitly, which gives

$$I_1 = -\frac{\alpha^2 + 2\alpha\beta}{\alpha^3} + \frac{e^{\alpha}}{\alpha^3}(\alpha^3\beta + \alpha^2 + 2\alpha\beta - 2\alpha^2\beta). \tag{15}$$

If $E_k = 0$, the field should be normalized using E_{k+1} and the procedure described above is repeated (see the Appendix).

Relation (13) containes a first-order correction to the original scheme (4). Both schemes are valid if (12) is satisfied. Condition (12) can be very restrictive. In the cathode region of the atmospheric pressure glow discharge [7] the electron temperature is about 10 eV and in order to increase the time step it is important to have a rather coarse grid in a high field region. Thus on a reasonable grid the electric field varies as $\simeq 10^4$ V/cm per cell. However, condition (12) gives $h_k \leq 10^{-4}$ cm, which is much less than any characteristic scale of the problem. To avoid this limitation an interpolation procedure is applied, as described below.

2.2. *Virtual Nodes*

The major idea of the scheme proposed is that in order to satisfy condition (11) two virtual nodes are inserted between x_k and x_{k+1} in such a way that the distance between them obeys (11) (Fig. 2). Densities at these nodes are obtained by interpolation of $n(x)$ on the interval (x_k, x_{k+1}) by some appropriate method. Then (13) or (4) is applied, where the number densities are replaced by their values at the virtual nodes.

Let some interpolation method be applied and, hence, one can calculate n at any point of the interval (x_k, x_{k+1}). We insert two virtual nodes with coordinates x_L and x_R between x_k and x_{k+1} (Fig. 2).

A space step limitation (11) now can be rewritten as

$$h_v \ll \frac{2D_{k+1/2}}{\mu|\Delta E_v|}, \tag{16}$$

where $h_v = x_R - x_L$ and

$$\Delta E_v = E_R - E_L = \frac{h_v}{h_k}\Delta E_k.$$

The distance between the virtual nodes h_v is chosen to satisfy condition (16). Introducing factor $\varepsilon \ll 1$, (16) can be rewritten as $h_v = \varepsilon 2D_{k+1/2}/(\mu|\Delta E_v|)$. Making simple algebraic manipulations it is easy to obtain

$$h_v = \sqrt{\varepsilon 2D_{k+1/2} h_k/\mu|\Delta E_k|}. \tag{17}$$

The virtual nodes are placed symmetrically around center point $x_{k+1/2} = \frac{1}{2}(x_k + x_{k+1})$ and, hence,

$$x_{L,R} = x_{k+1/2} \mp \tfrac{1}{2} h_v \tag{18}$$

$$E_{L,R} = E_{k+1/2} \mp \tfrac{1}{2}\Delta E_v, \tag{19}$$

where $E_{k+1/2} = (E_k + E_{k+1})/2$, minus corresponds to the subscript "L", and plus to "R," E_L and E_R being the field values at the virtual nodes. Interpolation is used to obtain the densities n_L and n_R in the virtual nodes x_L and x_R. To obtain $j_{k+1/2}$ expression (13) can be used where the k and $k + 1$ values should be replaced by the corresponding values at x_L and x_R. Moreover, if a distance between the virtual nodes satisfies condition (17), then (4) can be applied.

2.3. *Interpolation*

Two interpolation schemes have been used: exponential interpolation and local cubic piecewise (LCP) interpolation [8]. The exponential interpolation is constructed as follows. To prevent possible run-time errors it is better to interpolate $n + 1$ rather than n, as normally $n \gg 1$. At the interval (x_k, x_{k+1}) this gives

$$n(x) + 1 = (n_k + 1)e^{a(x - x_k)}, \quad a = \frac{1}{h_k}\log\left(\frac{n_{k+1} + 1}{n_k + 1}\right). \tag{20}$$

Alternatively, the method of [8] was used with the following modification. It has been found that the accuracy of LCP interpolation of rapidly changing functions is increased if one inter-

polates $\log(n(x) + 1)$ and then finds $n(x')$ as $\exp\{f_3(x')\} - 1$, where $f_3(x)$ is an piecewise cubic interpolation polynomial.

2.4. *Scheme Formulation*

Now we can summarize the results. In practice it is more convenient to express all the parameters in terms of drift velocity $W = -\mu E$ rather than E, as usually some approximation formula for $W(E)$ is available. Besides, field and velocity are usually known at the half-integer points. Making the appropriate transformations, the order of calculations with the scheme proposed is as follows:

1. Given the parameters at the two nodes k and $k + 1$ of the basic mesh, calculate the distance between the virtual nodes h_v using the relation

$$h_v = \sqrt{\varepsilon 2 D_{k+1/2} h_k / |W_{k+1} - W_k|}, \tag{21}$$

where $W_k = (W_{k+1/2} + W_{k-1/2})/2$. Here $\varepsilon \ll 1$ (typically 0.01–0.04) should be set (see further discussion). If $h_v \geq h_k$, $j_{k+1/2}$ is calculated by (4). Otherwise, the following procedure is used.

2. Define the positions of the virtual nodes x_L, x_R and the corresponding velocities:

$$x_{L,R} = \frac{x_k + x_{k+1}}{2} \mp \frac{h_v}{2} \tag{22}$$

$$W_{L,R} = W_{k+1/2} \mp \tfrac{1}{2} \Delta W_v, \tag{23}$$

where

$$\Delta W_v = \frac{h_v}{h_k}(W_{k+1} - W_k).$$

3. Define the densities n_L and n_R at the virtual nodes using interpolation (20) or [8] or another.

At this point there are two possible ways to calculate $j_{k+1/2}$. The simplest is to apply (4) on the interval (x_L, x_R), which we will refer to as the ISG-0 scheme,

$$j_{k+1/2} = \frac{D_{k+1/2}}{h_v I_0}(n_L - e^{\alpha_v} n_R) \tag{24}$$

where

$$\alpha_v = -\frac{h_v W_{k+1/2}}{D_{k+1/2}}, \quad I_0 = \frac{e^{\alpha_v} - 1}{\alpha_v}. \tag{25}$$

The more accurate approximation is obtained if one takes into account that the field is linear between the virtual nodes. This scheme, which will be referred as ISG-1 reduces to

$$j_{k+1/2} = \begin{cases} \dfrac{D_{k+1/2}}{h_v I_1}[n_L - e^{\alpha_v}(1 + \alpha_v \beta_v) n_R], & |W_L| \geq |W_R|, \\ \dfrac{D_{k+1/2}}{h_v I_1'}[e^{-\alpha_v'}(1 + \alpha_v' \beta_v')^{-1} n_L - n_R], & |W_L| < |W_R|, \end{cases} \tag{26}$$

where

$$\alpha_v = -\frac{h_v W_L}{D_{k+1/2}}; \quad \beta_v = \frac{W_R - W_L}{2W_L} \tag{27}$$

$$I_1 = \int_0^1 e^{\alpha_v y}(1 + \alpha_v \beta_v y^2)\, dy \tag{28}$$

$$\alpha_v' = -\frac{h_v W_R}{D_{k+1/2}}; \quad \beta_v' = \frac{W_R - W_L}{2W_R} \tag{29}$$

$$I_1' = \int_{-1}^0 e^{\alpha_v' y}(1 + \alpha_v' \beta_v' y^2)\, dy. \tag{30}$$

The explicit expressions for I_1 and I_1' are given by (15) and (42), respectively. If $W_k = W_{k+1} = 0$ a small nonzero field can be assigned to k node to prevent run-time error.

When the current density at the cell bound is found, one can calculate the number densities at the new time level using (5). This completes the description of the algorithm.

2.5. *Limit* $\varepsilon \to 0$

As has been shown, the only requirement which parameter ε in (21) should obey is $\varepsilon \ll 1$. To clarify the role of this parameter it is convenient to pass to the limit $\varepsilon \to 0$ or, equivalently, to the limit $h_v \to 0$ in expression for $j_{k+1/2}$ (24):

$$\lim_{h_v \to 0} j_{k+1/2} = \lim_{h_v \to 0}\left(\frac{D_{k+1/2}}{h_v I_0}(n_L - e^{\alpha_v} n_R)\right).$$

To calculate this limit we use the exponential interpolation (20). Taking into account (25) and the relations

$$n_L = (n_k + 1)\exp\{a(x_{k+1/2} - \tfrac{1}{2}h_v - x_k)\}$$

$$n_R = (n_k + 1)\exp\{a(x_{k+1/2} + \tfrac{1}{2}h_v - x_k)\},$$

we get

$$\begin{aligned} \lim_{h_v \to 0} j_{k+1/2} &= n_{k+1/2}(W_{k+1/2} - aD_{k+1/2}) \\ &= n_{k+1/2}\left(W_{k+1/2} - \frac{D_{k+1/2}}{h_k}\log\left(\frac{n_{k+1}+1}{n_k+1}\right)\right), \end{aligned} \tag{31}$$

where

$$n_{k+1/2} = (n_k + 1)e^{\alpha(1/2)h_k} = (n_k + 1)\sqrt{(n_{k+1} + 1)/(n_k + 1)}$$

and a is given by (20).

Evidently (31) is an approximation of the initial expression (2) for the current density with exponential interpolation of the number density at the cell bound. Each interpolation technique will lead to a similar expression. Scheme (31) is a high-order one with excessive dispersion which produces ripples on steep gradients (see further test results). These ripples are a well-known drawback of the high-order schemes.

We conclude that when ε changes from 0 to 1 scheme (24) transforms from a very accurate but dispersive one (31) to a less accurate, diffusive, but monotonic Sharfetter–Gummel algorithm (4).

3. TESTS

The quality of the numerical transport algorithm is usually demonstrated by the calculation of a given initial profile motion with the constant velocity. However, the advantages of the scheme proposed can be demonstrated only if the field (velocity) is not constant. In the case of a constant field the scheme considered is reduced to the original SG scheme. To check the scheme linear field

$$E(x) = Ax, \quad 0 \le x \le 1,$$

has been taken. Constant A, which defines the maximun field was taken to be 10^4. In this field the electron fluid moves towards $x = 0$ and suffers compression. Parameters μ and D were taken to be 1; thus $W = -Ax$. The equation to be solved is, therefore,

$$\frac{\partial n}{\partial t} - \frac{\partial (Axn)}{\partial x} - \frac{\partial^2 n}{\partial x^2} = 0. \tag{32}$$

The above set of parameters specify a convection-dominated problem which is a stringent test for the scheme proposed. To solve (32) we neglect the diffusion term in this equation. The convection equation

$$\frac{\partial n}{\partial t} - \frac{\partial (Axn)}{\partial x} = 0 \tag{33}$$

can be solved using the standard characteristic method which gives

$$n(x, t) = n_0(xe^{At})e^{At}. \tag{34}$$

Two initial profiles $n_0(x)$ were considered. The first is a model of the shock wave,

$$n_0(x) = n_1 + \frac{1}{2}\left[1 + \tanh\left(\frac{x - x_0}{\sigma}\right)\right] n_2, \tag{35}$$

where $\sigma = 0.02$. The second is a Gaussian profile,

$$n_0(x) = n_1 + n_2 \exp\left(\frac{(x - x_0)^2}{\sigma^2}\right) \tag{36}$$

with $\sigma^2 = 0.04$. In both cases $n_1 = 10^2$, $n_2 = 10^{12}$; thus the range of the n variation is 10 orders of magnitude.

All tests were performed using ISG-0 (24) and ISG-1 (26) schemes. Both ISG schemes are compared with the original Scharfetter–Gummel scheme (4) and the PHOENICAL SHASTA flux-corrected transport algorithm [9] with a Boris–Book flux limiter [10]. The exact solution (34) provides a basis for comparison.

Two uniform grids were used. The "fine" grid has 200 nodes, while the "coarse" grid has 100 nodes.

Figure 3a shows the motion of a "shock wave" when expo-

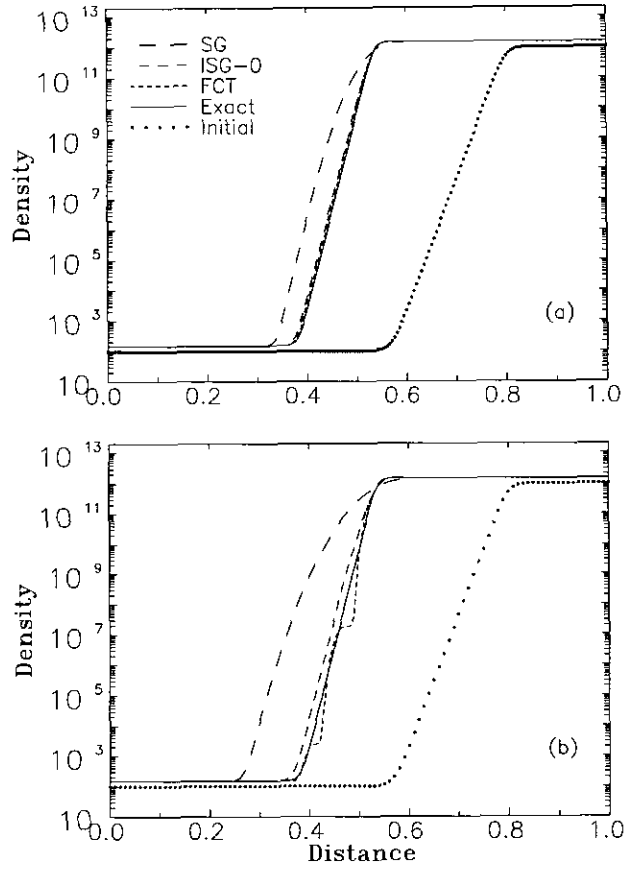

FIG. 3. (a) "Shock wave" transport in linear field $E = Ax$: 200 cells, Courant number 0.4, 200 time steps, $\varepsilon = 0.01$. SG—original Scharfetter–Gummel scheme (4), ISG-0—the scheme proposed, FCT—flux-corrected transport scheme [9]. The initial profile is plotted by gridpoints. (b) The same on the 100-cell grid, Courant number 0.2.

nential interpolation (20) is used. The fine grid is used (note that the initial profile is plotted by gridpoints); 200 time steps were performed with Courant number 0.4.

Figure 3b displays the result on the coarse grid. Again 200 time steps were performed with Courant number 0.2; thus it is with the same time step as in Fig. 3a. In both cases ISG-0 is used.

As is seen, the curves obtained by ISG-0 and FCT on the fine grid are almost identical and very close to the exact solution. In contrast, the original SG method gives a very diffusive solution which departs from the exact curve by several orders of magnitude. On the coarse grid FCT tends to produce a "staircase" on the profile, while ISG-0 preserves the monotonicity.

In Fig. 4a two interpolation methods are compared on a coarse grid. As is seen, when $\varepsilon = 0.01$ the scheme with exponential interpolation produces unphysical oscillations. With LCP interpolation the ISG-0 and ISG-1 curves merge together and both are monotonic. We conclude that LCP interpolation

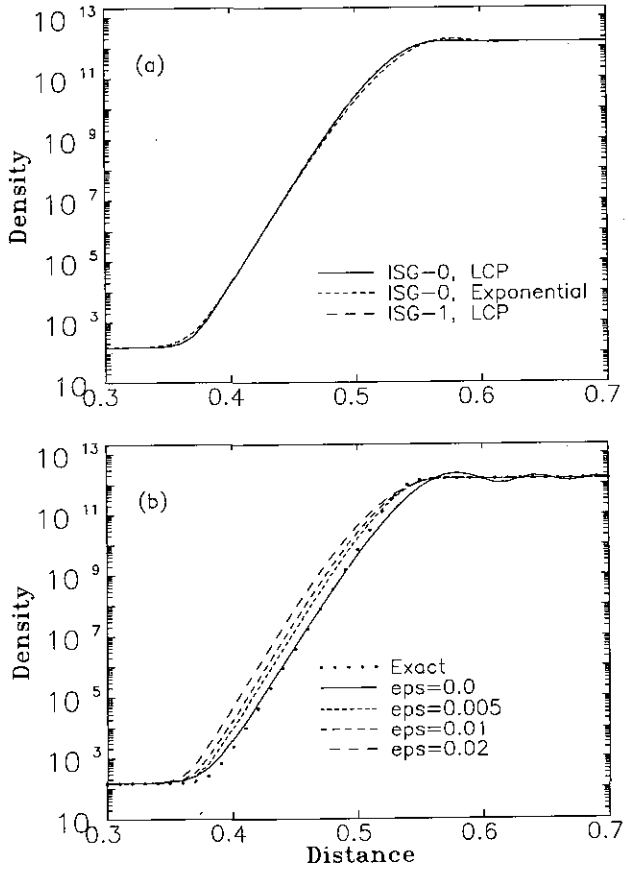

FIG. 4. The structure of "shock wave" profile. (a) Local cubic piecewise (LCP) interpolation is compared to exponential interpolation. The long-dashed curve obtained with (26) is merged to the solid line: 100 cells, Courant number 0.2, 200 time steps, $\varepsilon = 0.01$. (b) The influence of ε variation on the profile. If $\varepsilon = 0$ the scheme transforms to a high-order one which produces ripples. When ε is increased, the numerical solution departs from the exact one but becomes smooth.

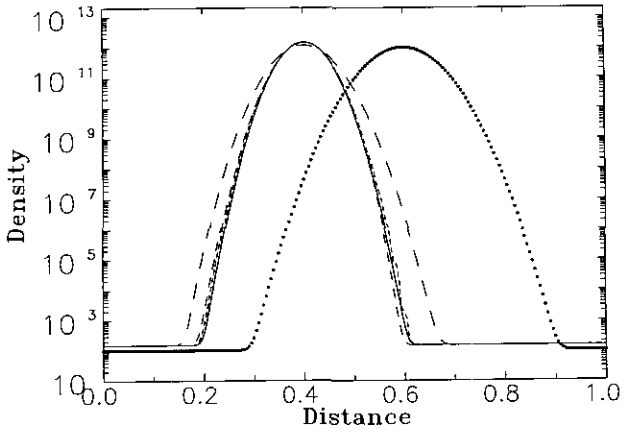

FIG. 5. Gaussian profile (dotted curve) transport; the notations and all the conditions are the same as in Fig. 3a.

is preferable and that the main benefit in accuracy gives introducing of the virtual nodes. Accounting for the linear field profile gives minor effect and thus (24) can be recommended.

Figure 4b shows the influence of the variation of ε in (21). When ε is increased, the ISG-0 solution tends to depart from the exact curve and approaches the original SG solution. When ε tends to zero, the ISG-0 transforms to a high-order scheme (as has been shown in Section 2.5) and ripples occur on a steep gradient (Fig. 4b).

On the other hand, if ε is fixed, $h_v \sim 1/\sqrt{|\Delta W|}$, where $\Delta W = W_{k+1} - W_k$. Therefore, if variation of the drift velocity within a cell is large, h_v becomes small, and vice versa. From this point of view, the scheme proposed acts similar to the flux-corrected transport technique; it is less diffusive in a region of high gradient of a drift velocity, and more diffusive when ΔW became small. In real physical problems a high gradient of the electron drift velocity is inherently related to a high gradient of the particle number density and, hence, one might expect the variable h_v to prevent the production of unphysical ripples on a density profile.

The analysis presented above leads to the limitation $\varepsilon \ll 1$, but the actual value of this parameter should be chosen experimentally. Our experience shows that ε from the range 0.01–0.04 gives good results in most cases.

Figure 5 shows the motion of Gaussian profile on the fine grid. LCP interpolation is used. Again the results obtained by FCT and ISG-0 are close to each other and to the exact solution.

The tests performed show that the accuracy of the scheme proposed is comparable to one of the best transport schemes—FCT. ISG does not produce a "staircase" on steep gradients. The additional advantage of ISG is that it takes into account both convection and diffusion simultaneously.

The scheme is simple and easy to implement. Special tests have been done to estimate the efficiency of this scheme. The results have shown that the rates of calculations with ISG and

FCT are almost the same. However, we believe that ISG will be much faster on computers equipped with hardware-supported calculation of exponents.

The accuracy of the scheme depends on ε and on the interpolation procedure applied. Generally, more sophisticated LCP interpolation gives better results than simple exponential interpolation. However, the latter provides good result if the grid is "fine" enough.

In conclusion it should be mentioned that this scheme was succsessfully used in quasi-1D and 2D simulation of streamer dynamics in air. The feature of this problem is a very large gradient of the electric field in the streamer "head." Nevertheless, the scheme proposed has given a stable and accurate solution on a reasonable grid. The results of this work will be published elsewhere.

APPENDIX

If $E_k = 0$, the field (6) should be represented as

$$E(x) = E_{k+1}(1 + 2\beta'\eta), \tag{37}$$

where $\eta = (x - x_{k+1})/h_k$ and

$$\beta' = \frac{E_{k+1} - E_k}{2E_{k+1}} = \frac{\Delta E_k}{2E_{k+1}}. \tag{38}$$

Then the procedure described in Subsection 2.1 is repeated, leading to the expression for $j_{k+1/2}$,

$$j_{k+1/2} = \frac{D_{k+1/2}}{h_k I_1^l(\alpha', \beta')}[e^{-\alpha'}(1 + \alpha'\beta')^{-1}n_k - n_{k+1}], \tag{39}$$

where

$$\alpha' = \frac{\mu h_k E_{k+1}}{D_{k+1/2}} \tag{40}$$

and

$$I_1^l(a, b) = \int_{-1}^{0} e^{ay}(1 + aby^2)\, dy \tag{41}$$

$$= \frac{a^2 + 2ab}{a^3} - \frac{e^{-a}}{a^3}(a^3b + a^2 + 2ab + 2a^2b). \tag{42}$$

ACKNOWLEDGMENT

The author is grateful to the referees, who proposed the idea to pass to the limit $\varepsilon \to 0$, which helps to clarify the mechanism of the scheme considered.

REFERENCES

1. E. Oran and J. P. Boris, *Numerical Simulation of Reactive Flow*, (Elsevier, Amsterdam, 1987).
2. D. L. Scharfetter and H. K. Gummel, *IEEE Trans. Electron Devices* **ED-16,** 64 (1969).
3. Yu. A. Berezin, and M. P. Fedoruk, *Numerical Simulation of Nonstationary Processes in Plasmas,* (Nauka, Novosibirsk, 1993), p. 317. [Russian]
4. M. Kurata, *Numerical Analysis for Semiconductor Devices* (Heath, Lexington, MA, 1982).
5. J.-P. Boeuf and L. C. Pitchford, *IEEE Trans. Plasma Sci.* **19**(2), 286–296 (1991).
6. A. Fiala, L. C. Pitchford, and J.-P. Boeuf, *Phys. Rev. E* **49**(6), 5607 (1991).
7. A. A. Kulikovsky, *J. Phys.D: Appl. Phys.* **26,** 431 (1993).
8. M. Davis and J. Dowden, *Computing* **38**(4), 299 (1987).
9. R. Morrow and L. E. Cram, *J. Comput. Phys.* **57,** 129 (1985).
10. J. P. Boris and D. L. Book, *J. Comput. Phys.* **20,** 397 (1976).